Featured in Physics

Stable and High-Quality Electron Beams from Staged Laser and Plasma Wakefield Accelerators

F. M. Foerster[1,*] A. Döpp[1,2,†] F. Haberstroh[1] K. v. Grafenstein,[1] D. Campbell,[1,3] Y.-Y. Chang,[4] S. Corde[5]
J. P. Couperus Cabadağ[4] A. Debus[4] M. F. Gilljohann,[1,5] A. F. Habib,[3] T. Heinemann[3,6] B. Hidding,[6,3] A. Irman[4]
F. Irshad,[1] A. Knetsch[5] O. Kononenko[5] A. Martinez de la Ossa[7] A. Nutter,[4,3] R. Pausch,[4,8] G. Schilling,[1]
A. Schletter,[1,9] S. Schöbel,[4,8] U. Schramm[4,8] E. Travac,[1] P. Ufer,[4,8] and S. Karsch[1,2,‡]

[1]*Ludwig-Maximilians–Universität München, Am Coulombwall 1, 85748 Garching, Germany*
[2]*Max Planck Institut für Quantenoptik, Hans-Kopfermann-Strasse 1, 85748 Garching, Germany*
[3]*University of Strathclyde, 107 Rottenrow, Glasgow G4 0NG, United Kingdom*
[4]*Helmholtz-Zentrum Dresden-Rossendorf, Bautzner Landstrasse 400, 01328 Dresden, Germany*
[5]*Laboratoire d'Optique Appliquée, ENSTA Paris, CNRS, Ecole Polytechnique,*
Institut Polytechnique de Paris, 91762 Palaiseau, France
[6]*The Cockcroft Institute, Keckwick Lane, Warrington WA4 4AD, United Kingdom*
[7]*Deutsches Elektronen-Synchrotron DESY, Notkestr. 85, 22607 Hamburg, Germany*
[8]*Technische Universität Dresden, 01062 Dresden, Germany*
[9]*Technische Universität München, James-Franck-Strasse 1, 85748 Garching, Germany*

We present experimental results on a plasma wakefield accelerator (PWFA) driven by high-current electron beams from a laser wakefield accelerator (LWFA). In this staged setup stable and high-quality (low-divergence and low energy spread) electron beams are generated at an optically generated hydrodynamic shock in the PWFA. The energy stability of the beams produced by that arrangement in the PWFA stage is comparable to both single-stage laser accelerators and plasma wakefield accelerators driven by conventional accelerators. Simulations support that the intrinsic insensitivity of PWFAs to driver energy fluctuations can be exploited to overcome stability limitations of state-of-the-art laser wakefield accelerators when adding a PWFA stage. Furthermore, we demonstrate the generation of electron bunches with energy spread and divergence superior to single-stage LWFAs, resulting in bunches with dense phase space and an angular-spectral charge density beyond the initial drive beam parameters. These results unambiguously show that staged LWFA-PWFA can help to tailor the electron-beam quality for certain applications and to reduce the influence of fluctuating laser drivers on the electron-beam stability. This encourages further development of this new class of staged wakefield acceleration as a viable scheme toward compact, high-quality electron beam sources.

Subject Areas: Optics, Particles and Fields
Plasma Physics

I. INTRODUCTION

Laser wakefield acceleration (LWFA) is a promising high-gradient accelerator technology. It uses intense beams of light to generate strong *wakefields* in a plasma for the acceleration of electrons [1,2]. In LWFA, the ponderomotive force of the laser strongly displaces the plasma electrons from their equilibrium position around the much heavier ions. This displacement causes large charge separation fields behind the laser as it traverses the plasma with a velocity close to the speed of light. The magnitude of these wakefields is of the order of the cold wave breaking field $E_0 = m_e c \omega_p / e \approx 96 \, \text{GV m}^{-1} \times \sqrt{n_e [10^{18} \, \text{cm}^{-3}]}$. Here m_e denotes the electron rest mass, c is the speed of light, ω_p is the plasma frequency, e is the elementary charge, and n_e is the plasma electron density. At densities around 10^{18} cm^{-3} the acceleration gradient in these accelerators is thus several orders of magnitude higher than the breakdown fields in conventional radio frequency (rf) accelerators ($\sim 100 \, \text{MV m}^{-1}$), allowing for a significant downsizing of the accelerator. LWFA experiments are routinely performed at numerous high-power laser facilities [3–11] and reach high charge ($\sim$nC) [12,13] combined with

an ultrashort bunch duration ($\sim$10 fs) [14,15], resulting in high peak currents of tens of kiloampere [13,16]. Furthermore, the bunches typically have a few-micrometer source size at the exit of the accelerator [17–19], which is paired with few-millirad divergence [12,20].

One of the most exciting prospective applications of these accelerators is their use for driving a compact free-electron laser (FEL) [21]. Similarly, they may form the basis for future compact particle colliders. However, some limitations of the technology have so far prevented a real breakthrough in these and other applications. Firstly, as a consequence of the very high acceleration gradients [22] and their reliance on nonlinear laser propagation [23,24] small parameter jitters result in large shot-to-shot fluctuations of the electron energy. Thus, it is extremely challenging for LWFAs to reach an energy stability and energy spread comparable to conventional rf accelerators. Secondly, the normalized emittance of LWFA electron beams appears to be limited to around 0.1–1 mm mrad [25–27], likely due to heating of plasma electrons by the intense drive laser, spatiotemporal asymmetries in the driver, or the interactions of electrons and the trailing laser fields during acceleration. While significant progress has been made over the past years, including the demonstration of first gain in an LWFA-driven FEL [21] and stable long-term operation by actively controlling laser parameters [28], it will remain difficult to solve all of these problems simultaneously. The generation of low-emittance beams will be particularly difficult in proposed multistage LWFA concepts for high-energy physics [29]. In such schemes, the plasma mirrors needed for coupling in multiple laser beams will cause the emittance to increase [30].

LWFA's particle-driven counterpart, plasma wakefield acceleration (PWFA), relies on the Coulomb field of a relativistic drive beam and can potentially mitigate some of these problems [31]. In particular, it has been suggested that ultralow-emittance beams can be internally injected into a beam-driven wakefield [32–34]. Nonetheless, PWFA remains less common due to its reliance on high-current drive beams of electrons [35–37] or protons [38], which were until now only available at a few large-scale accelerator facilities. This situation has changed recently, as we demonstrated that high-current LWFA electron beams are also well suited to drive strong plasma waves, even in high-density plasmas [39]. These in turn can accelerate witness bunches at gradients of around 100 GeV/m [40]. This possibility opens up a new approach in high-gradient accelerator research, namely, using LWFA electron beams to drive a PWFA and to internally inject a high-quality beam into the PWFA. While the staging of two plasma-based acceleration methods may sound like an unnecessarily complex approach, we discuss in this article how the method can efficiently combine the strengths and mitigate the weaknesses of each individual scheme. In particular, our experimental results validate the potential of employing

an extra PWFA stage with internal injection to improve the electron quality over the output of a single LWFA.

The paper is structured as follows. First, we introduce a new all-optical injection scheme for density down-ramp injection in the PWFA stage. In a first experiment this new setup is used to investigate the stability of the PWFA stage. We demonstrate stable production of electron beams from a staged LWFA-PWFA, with the PWFA stage reaching an energy stability comparable to the drive beam produced in the LWFA stage. Simulations indicate that the intrinsic insensitivity of PWFA to the energy of the drive beam may even allow for using the PWFA stage as a stability transformer, i.e., a system that improves upon the energy stability of a single LWFA stage. In a second experiment, we inject a witness beam in an optically generated density down ramp in the PWFA stage to achieve a superior electron beam quality ("quality transformer"). We demonstrate experimentally that its energy spread and divergence beat the respective quantities of its drive bunch, resulting in a net gain in angular-spectral charge density [41].

II. EXPERIMENTAL SETUP

We have performed a series of closely related experiments on staged LWFA-PWFA. The basic setup is illustrated in Fig. 1. To address various aspects of the staging scheme the PWFA parameters are varied. A summary of the PWFA setups presented in this article is given in Table I.

Laser.—The laser wakefield accelerator is driven by the ATLAS laser system at the Centre for Advanced Laser Applications in Garching, Germany. During the experiment ATLAS delivered laser pulses with (5 ± 1) J on target [43] with 30 fs (FWHM) duration at a central wavelength of 800 nm. The laser beam is focused in an $f/33$ geometry, reaching a peak intensity of $(1.3 \pm 0.3) \times 10^{19}$ W/cm^2, which corresponds to a normalized vector potential of $a_0 = 2.5$.

Target.—The laser is focused onto a target consisting of a first and a second gas jet [see Fig. 1(a)], doubling as the LWFA and PWFA stages, respectively. Both jets are separated by a 10-mm-wide vacuum gap, where diffraction reduces the driver intensity enough to prevent the excitation of any significant wakefield in the PWFA stage. Additionally, a tape drive can be inserted between the jets to completely block the laser, which also prevents ionization of the second jet. In this case, an additional low-energy laser beam can be used to preionize the PWFA stage.

The LWFA stage uses a 5 mm Laval nozzle fed with a 96∶4 (molecule ratio) mixture of hydrogen and nitrogen gas. The 4-mm-long PWFA stage uses either pure hydrogen or mixtures of hydrogen and helium, depending on the specific setup. Both jets' density profiles are discussed in the Supplemental Material [42]. The LWFA is operated at a plateau plasma density of $(1.4 \pm 0.1) \times 10^{18}$ cm^{-3}, whereas the PWFA stage is operated at peak densities between $(1-2) \times 10^{18}$ cm^{-3} [44]. In the LWFA stage, the
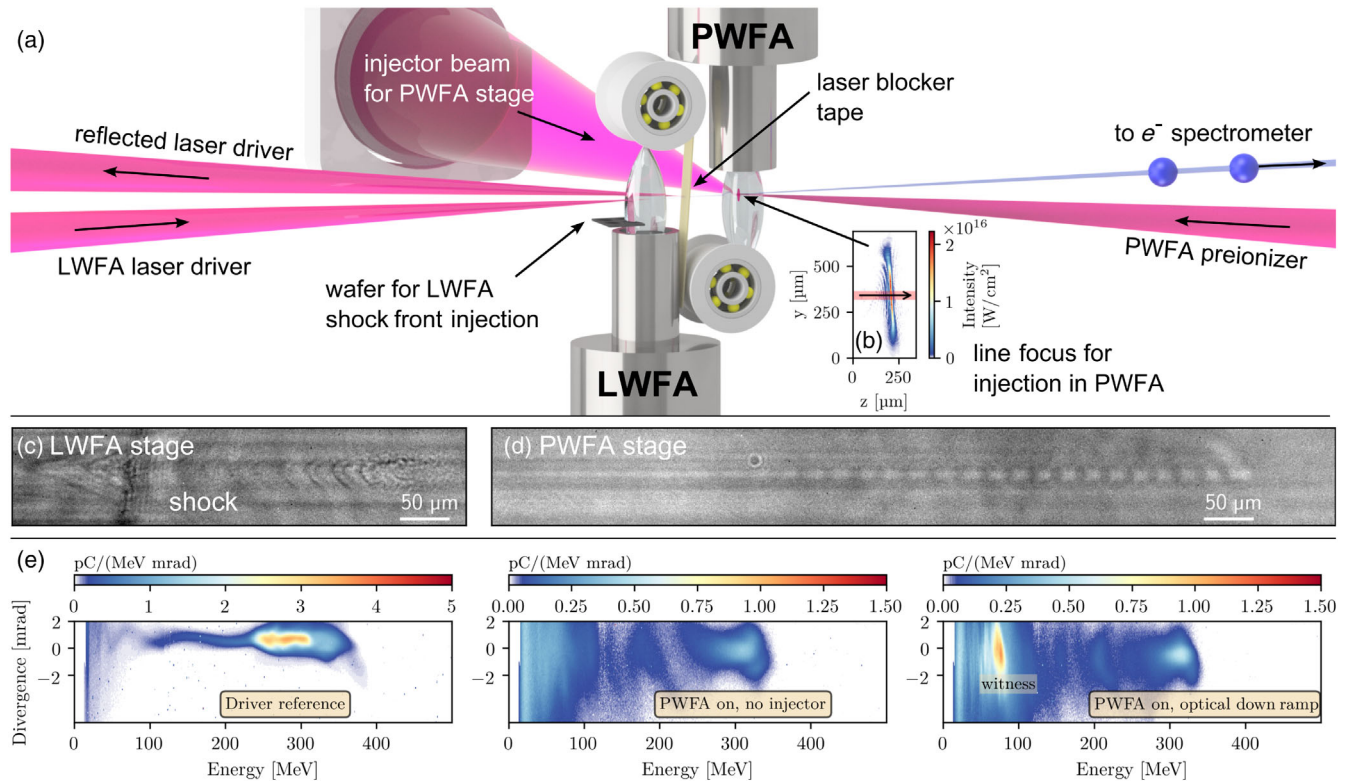
FIG. 1. Experimental setup for staged LWFA-PWFA with internal injection in the PWFA stage. (a) Schematic of the double-jet setup for staged LWFA-PWFA experiments. In the first plasma, the drive pulse propagating along the z axis generates LWFA electrons via shock-front-assisted ionization injection. A 25-μm-thick polyimide tape after the first jet prevents the laser from ionizing the second jet for the first set of experiments. An astigmatic laser focus oriented perpendicular to the wakefield axis (b) heats the plasma in the PWFA stage a few nanoseconds before the electron driver arrives. A pair of planar plasma density shocks evolves. The second shock provides the down ramp for the injection of witness electrons into the PWFA stage. A few-cycle probe was used to image the laser-driven plasma wave in the LWFA stage (c) and the electron-driven plasma wave in the PWFA stage (d). Typical spectra (e) of the electron beam from the LWFA stage, the spent drive beam after the PWFA stage without injection, and an internally injected witness beam are shown. Without injector laser beam only a broadband background of decelerated LWFA electrons is formed in the PWFA stage. With injector beam the witness is the defined peak on top of this background at around 70 MeV.

hydrodynamic shock front originating from a silicon wafer edge obstructing the supersonic gas flow triggers shock-front-assisted ionization injection [45] [see Fig. 1(e)] to create the drive bunch for the subsequent PWFA stage.

Injector beam.—In contrast to previous works using a wire-generated hydrodynamic density down ramp [46], we introduce hydrodynamic optically field-ionized (HOFI) plasma gradients [47,48] to facilitate electron injection in

TABLE I. Summary of experimental conditions.

Figure(s)	1 and 2	4(a) and 4(b)	4(c) and 4(d)
Driver charge	(340 ± 46) pC	(657 ± 61) pC	(461 ± 99) pC
Driver energy	(287 ± 18) MeV	(235 ± 14) MeV	(284 ± 30) MeV
Driver divergence (FWHM, no laser blocker, no second jet)	(1.1 ± 0.2) mrad	(0.9 ± 0.1) mrad	(4.4 ± 0.5) mrad
Gap between stages	1 cm	$(1–1.9)$ cm	1.25 cm
Nozzle PWFA	4 mm	7 mm	4 mm
Gas PWFA	$50\% \, H_2 + 50\% \, He$	H_2	H_2
Density PWFA	$(2.0 \pm 0.2) \times 10^{18}$ cm^{-3}	$(1.1 \pm 0.2) \times 10^{18}$ cm^{-3}	$(2.0 \pm 0.2) \times 10^{18}$ cm^{-3}
Down-ramp generation	Optically	Optically	Wire
Laser blocker tape	25 μm (Kapton)	No	No
Preionizer	On	Off	Off

the PWFA stage. In this scheme a transversely propagating laser locally ionizes and heats the plasma, forming a plasma channel associated with a hydrodynamic shock structure. In contrast to other groups' work [49–51], which suffered from alignment sensitivity and pointing jitter, our use of a strongly astigmatic focus [Fig. 1(b)] ensures the formation of two nearly planar shocks perpendicular to the main laser axis. Their large area makes this setup very insensitive to alignment errors and ensures high stability [52]. Our optically induced down ramps for injection enable us to tailor the shape, height, and gradient of the plasma density down ramp independently of the gas density or the nozzle geometry. The relative delay between the injector laser beam and the arrival of the electron beam can be adjusted between (0–2) ns. Together with the energy of the injector laser pulse this permits us to adjust the parameters of the HOFI shock [47] and, thus, the plasma density down ramp for injection. In our experiment witness bunches are reliably injected at 1.3 ns delay and a peak intensity of the injector laser beam of 2×16 W/cm^2 [Fig. 1(b)]. This added flexibility decouples injection and acceleration in the PWFA stage. In particular, by setting the correct orientation of the astigmatic focus, the shock can be created perpendicular to the beam axis, crucial for the generation of high-quality witness beams [53,54] and hard to achieve with supersonic shock formation. In addition, the position jitter of the HOFI injector is only a few micrometers and smaller than typically achieved with wire-generated shocks [42].

Diagnostics.—The main diagnostic in this experiment is a 0.8-m-long dipole spectrometer, placed 2.9 m downstream of the target. Electrons are deflected onto a calibrated scintillator screen [55], whose emission is imaged onto a 12-bit CMOS camera. The spectrometer covers an energy range from 12 MeV onward, with transverse angular acceptance range of ± 6 mrad.

III. STABLE STAGED ACCELERATION

In a first experiment, we investigate the energy stability of the witness injected in the PWFA stage. In this experiment we operate the PWFA stage with a 1:1 mixture of hydrogen and helium (molecule ratio). The laser blocker tape was used to ensure a purely beam-driven wakefield in the second stage.

The LWFA-generated drive bunches in this experiment have a peak energy of (287 ± 18) MeV (SD). Taking into account all electrons with an energy above 200 MeV, we measure a charge of (340 ± 46) pC (14%, SD); see also Fig. 1(e) (left). Once the beam traverses the second jet (preionizer on, but without injector) the electrons are decelerated and we observe a broadband electron spectrum; see Fig. 1(e) (middle).

When the injector is activated, a witness bunch is injected at the optically generated shock front in the PWFA stage. The witness spectra exhibit a distinct energy
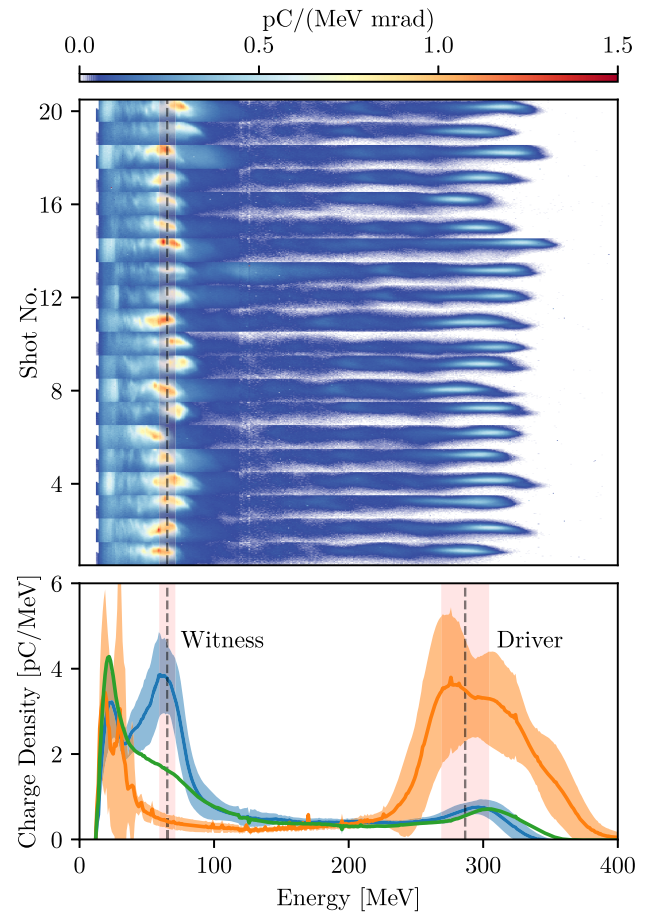

FIG. 2. Experimental data on stable plasma wakefield acceleration. Top: output spectra of 20 consecutive shots with the HOFI-generated shock and preionized plasma in the second jet. Bottom: electron spectra with injector laser beam (blue). This is compared to spectra without plasma (orange) and with plasma, but no injector (green) in the PWFA stage. The strong charge and energy loss of the driver in the green case and the injection of a high-charge witness in the blue case are evident. Dashed lines and red shaded areas indicate the mean of the energy and its standard deviation of driver and witness bunches, respectively. For reference, angle-resolved spectra of the drive beam alone and after the PWFA stage but without injector can be found in Fig. 1.

peak. Furthermore, we observe that the witness injection is very reproducible and, as shown in Fig. 2, the energy of the spectral peak fluctuates only within (65 ± 6) MeV (9%, SD). Thus, the absolute fluctuation (red shaded area in Fig. 2) of the witness peak energy is only one third of the drivers and they are comparable in terms of their relative energy jitter. The charge of the witness beam is (59 ± 19) pC (SD). In terms of energy stability we thus already achieve a performance that is comparable [56] or even superior [57] to recent experiments on all-optical density down-ramp (Torch) injection at large-scale rf-accelerator-driven PWFAs.

This high stability of the witness energy in our staged LWFA-PWFA appears surprising at first because of the

much higher shot-to-shot fluctuations of the LWFA-generated driver as compared to a drive beam from a conventional accelerator. The insensitivity of the witness energy to the driver energy and energy spread can be understood from the expression for the Coulomb field of a highly relativistic ($\gamma \gg 1$), axially symmetric electron beam. Assuming that the beam is contained within a radius r_0, the field at a transverse distance $r > r_0$ is given by

$$\vec{E}_b(\zeta, r) = -\frac{I(\zeta)}{2\pi\epsilon_0 c}\frac{\vec{e}_r}{r}, \qquad (1)$$

with $I(\zeta)$ the current profile of the beam in the comoving variable $\zeta = z - ct$, ϵ_0 the vacuum permittivity, and c the speed of light. We can see from Eq. (1) that the electric field responsible for setting up the plasma wave is purely oriented in the transverse direction and does not depend on the electron energy. For sufficiently narrow and high-current beams ($I \gtrsim 1$ kA), the Coulomb field strongly expels all plasma electrons from its path leaving behind a homogeneous and symmetric ion column. The plasma electrons are attracted back by the space charge field of the ion column, $E_{\text{ion}}(r) = -en_0 r/2\epsilon_0$, and start oscillating radially, forming a sheath around the ensuing ion cavities. The maximal radial position of the sheath is usually referred to as the *blowout radius*. A useful scaling of the blowout radius r_b can be obtained by calculating the radial distance at which the electrostatic force of the ion background cancels out that of the drive beam. Evaluating Eq. (1) at the point of maximum current I_0 we obtain

$$r_b \simeq \sqrt{I_0/\pi ecn_0} \propto \sqrt{I_0/n_0}. \qquad (2)$$

Note that by balancing electrostatic fields we implicitly restrict the validity of the model to slow plasma electrons in the sheath, for which the Lorentz force is essentially given by the electric field [58]. To estimate the accelerating field we use the notion that, in case of a strong blowout, the plasma sheath approximates a sphere and the longitudinal electric field inside the ion cavity decreases linearly from the cavity center with a slope $\partial_\zeta E_z \simeq en_0/2\epsilon_0$ [60]. Thus, evaluating E_z at a distance r_b from the cavity center, we obtain for the maximum accelerating field:

$$E_z^{\text{max}} \simeq -en_0 r_b/2\epsilon_0 \propto -\sqrt{I_0 n_0}. \qquad (3)$$

For small deviations the derived square-root scaling [Eq. (3)] predicts that the relative deviation of the longitudinal electric field is half of the relative deviation of both beam current and plasma density. To compare the scaling to our experiment it is assumed that the drive bunch length is constant. Thus, the charge of the drive beam is proportional to its beam current and the 14% driver charge fluctuation translates into 7% variation of the witness beam energy. Furthermore, we observe an imperfect regulation of the

backing pressure for the PWFA stage leading to a density jitter of $\pm 4\%$ (SD). This translates into 2% energy jitter of the witness beam energy. Further assuming both error contributions to be independent and normally distributed, we expect an energy jitter of 5 MeV for our current setup. Thus, the prediction of the simplified model on the stability of the staged LWFA-PWFA is consistent with the measured energy of (65 ± 6) MeV.

The ratio of the relative fluctuations of witness energy $\delta E_{\text{witness}}$ and driver charge δQ_{driver} can be understood as a measure for the resilience of the PWFA stage to variations of the driver. The measured value of $|\delta E_{\text{witness}}[\%]| \leq 0.68 |\delta Q_{\text{driver}}[\%]|$ [61] which is smaller than 1 indicates a damping behavior.

In future experiments, the intrinsic insensitivity of the PWFA stage to the energy of the drive beam may even permit us to increase the energy stability of a staged LWFA-PWFA beyond that of the LWFA alone. We have modeled the scenario of density down-ramp injection in a plasma wakefield accelerator stage using the quasi-3D particle-in-cell (PIC) code FBPIC [62]. As shown in Fig. 3(a), the input parameters are similar to our experiment (for details, see Supplemental Material [42]).

In a first set of 100 simulations we model the experimentally observed drive bunch in terms of average charge and energy and their random variations (mean and standard deviation as in the experiment). As shown in Fig. 3(c) the mean energy of the witness bunch is 165 ± 7 MeV (SD), and $|\delta E_{\text{witness}}[\%]| \leq 0.34 |\delta Q_{\text{driver}}[\%]|$. Thus, the relative energy variation of the simulated witness is smaller than in the experiment.

We study the reason for this finding in independent scans of driver energy and charge. First, we vary the driver energy between half and 8 times the value of the experiment, while keeping the driver charge constant at 340 pC. Beyond a certain energy level, which is on the order of 200 MeV for our simulation parameters, depletion of the driver can be neglected [see Fig. 3(d)]. As follows from Eq. (1), the wakefield strength does not depend on the driver's electron energy and thus the witness energy stays constant. This finding holds for a broad driver energy range that far exceeds the measured energy fluctuations in our experiment (the latter are highlighted in orange).

In a second set of simulations we scan the driver charge between 240 and 440 pC while keeping the energy constant at 287 MeV. In these simulations the mean witness energy slightly decreases with increasing driver charge around the experimental working point ($\delta E_{\text{witness}}[\%] = -0.35 \, \delta Q_{\text{driver}}[\%]$). Furthermore, the spectrum broadens toward stronger drivers. This downshift and broadening of the spectra can be explained with beam loading of the wakefield. In the simulations the injected charge is positively correlated to the driver charge [Fig. 3(e)]. Thus, the amount of injected charge can attenuate, or even overcompensate the higher energy gain
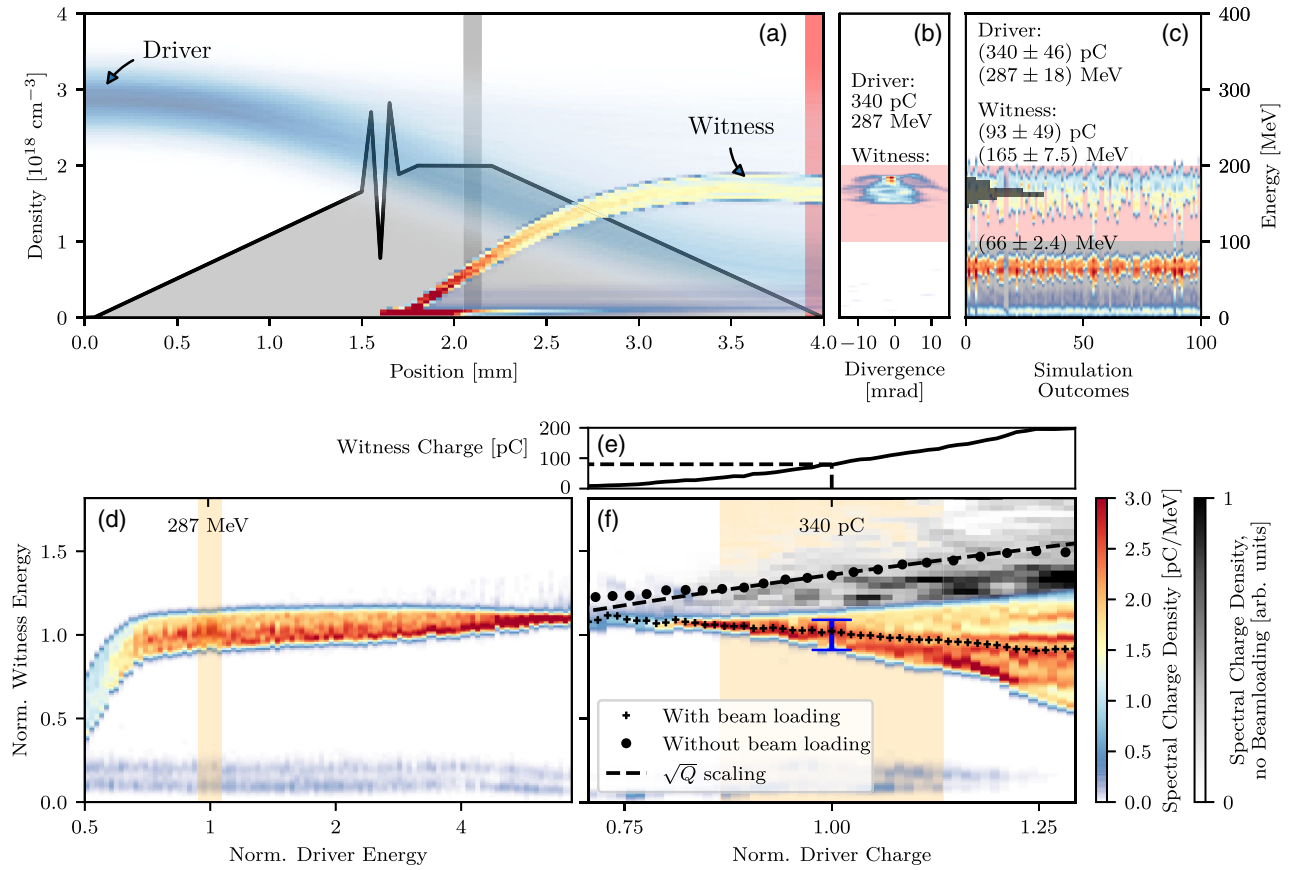
FIG. 3. PIC simulations on stable staged acceleration. (a) Modeled density distribution and evolution of driver and witness energy in the PWFA stage. (b) Angular-resolved witness spectrum for the experimental driver parameters. (c) Set of 100 simulations with randomized variation of driver charge and energy with standard deviation as in the experiment. For comparison the spectra of an earlier simulation step [gray shaded in (a)] are shown where the energy gain resembles the experimental outcome. Panels (d) and (f) show the spectral charge density of the witness for parameter scans of the driver energy and charge. Given that driver depletion can be neglected (here driver energy > 200 MeV), the witness energy does barely depend on the driver energy. Panel (f) shows the spectral charge density of the witness bunch (color scale and black crosses) as a function of the driver charge. With increasing driver charge the witness charge increases (e), the witness spectrum broadens, and its mean energy slightly decreases. For comparison the energy gain of a test bunch in an unloaded wakefield with equal driver is plotted (gray scale and black dots). In both scans the experimental working point is indicated by the orange shaded area. The simulation outcome in (d) and (f) is normalized to the experimental working point in (b). For comparison the experimental standard deviation of the witness energy is plotted in blue. Note that the experimental result is normalized independently.

expected for stronger drive beams in the PWFA via beam loading.

To quantify this effect we include a species of test particles in the PIC simulations to sample the longitudinal phase space. We then compare the energy gain of the witness in the case of a beam loaded and an unloaded wakefield (method described in the Supplemental Material [42]). In Fig. 3(f) both cases are compared. The mean witness energy in the hypothetical unloaded case roughly follows the $\sqrt{Q}$ scaling for the longitudinal wakefield strength as a function of the driver charge ($\delta E_{\mathrm{witness}}[\%] = +0.48\,\delta Q_{\mathrm{driver}}[\%]$). In the experiment the injected witness charge is expected to fluctuate not only as a function of the driver charge, but also due to other parameters that were kept constant in the simulations (e.g., gas density

distribution, down-ramp gradient, and height). Thus, a random contribution to the witness energy, depending on the magnitude of the additional witness charge variation, is added and $|\delta E_{\mathrm{witness}}/\delta Q_{\mathrm{driver}}|$ must be expected to be higher than in the simulations. Note that the sign of $\delta E_{\mathrm{witness}}/\delta Q_{\mathrm{driver}}$ is not experimentally observable because the PWFA stage deletes the information about the initial driver charge. Thus, only mean and standard deviation of driver and witness charge [orange shaded area and blue bar in Fig. 3(f)] of similar runs can be compared and correlations as in Fig. 3(f) cannot be revealed in the experiment.

The mean energy of the witness beam in the simulations is 2.5 times higher as compared to the experiment. While this experiment was not optimized for highest energy, but highest stability, the main reason for this discrepancy might

be that the wakefield strength is overestimated in our simulations. The drive bunch is initiated without taking the interaction at the laser blocker tape into account. Simulations showing the influence of the driver emittance on the witness beam and a discussion of the angular distribution of the witness beam can be found in the Supplemental Material [42].

The beams presented in Fig. 2 do not only exhibit high energy stability, but they also carry a significant fraction of the energy of the LWFA-generated drive bunch. We calculate the overall energy transfer efficiency as the ratio of the integrated energy of the incident LWFA-generated driver bunch (E_{driver}) and energy gain of the PWFA witness bunch ($\Delta E_{\text{witness}}$) according to following definition [63]:

$$\eta = \frac{\Delta E_{\text{witness}}}{E_{\text{driver}}}, \qquad (4)$$

For data from Fig. 2, we find $E_{\text{driver}} = (102 \pm 14)$ mJ and $\Delta E_{\text{witness}} = (4 \pm 1)$ mJ, which thus yields an overall efficiency from incident driver to witness of $\eta = 4\%$ and, for some experimental conditions [64], this efficiency reaches up to 10%. This is at least a factor of 2 more than shown in experiments with either external [36,37,65] or internal [40,56,57] injection and, to our knowledge, the highest total driver to witness energy transfer efficiency observed for a PWFA to date.

As we discuss in the following section, the hybrid approach not only reaches a substantial energy transfer efficiency, but can also lead to a net improvement of selected beam parameters.

IV. HIGH-QUALITY ELECTRON BEAMS FROM STAGED ACCELERATION

As discussed, a staged LWFA-PWFA helps to decouple the electron energy from shot-to-shot fluctuations of the driver bunch. The established stability of the wakefield in combination with a controlled injection enables the pursuit of a beam-quality transformer [66]. As a figure of merit we use the angular-spectral charge density, i.e., the charge per solid angle ("angular") and energy interval ("spectral"). We define it as the spectrally resolved charge within the rms divergence divided by the solid angle corresponding to this divergence [67]. To deduce the solid opening angle rotational symmetry of the witness bunches is assumed. Experimental evidence for an overall improvement regarding the electron-beam density is presented in the following section.

For this demonstration, the laser blocker tape between both acceleration stages was removed. By that we avoid additional emittance growth of the drive beam due to the Weibel instability [30]. The resulting lower emittance of the driver results in a denser drive bunch in the PWFA stage. These unperturbed drive beams are expected to generate a stronger and more symmetric blowout, which is crucial for

the generation of high-quality witness beams [68]. Similar to previous experiments [12,40], in order to exclude the laser beam as the dominating driver of the second stage a distance ≥ 1 cm between both jets is chosen. Figure 4(a) shows a typical drive bunch generated by our 150-TW LWFA for this set of experiments. The average charge in a set of 30 shots was (657 ± 61) pC (SD) in the high-energy feature at 250 MeV. The shot shown in Fig. 4 has a charge of 640 pC in the high-energy feature and its average divergence is 0.41 mrad (rms of super-Gaussian fit; for details see Supplemental Material [42]). The angular-spectral charge density is 5 pC/(MeV μsr) [69].

In our experiment, we are able to modify the density down ramp for injection in the PWFA stage by tuning the delay, intensity, and position of the injector laser pulse and thus independently of the gas density, gas species, and nozzle profile. With the millirad-level divergence of the LWFA-generated bunch, the distance between LWFA and PWFA stage serves as a parameter to adjust the density of the drive bunch when entering the second stage. Thus, the drive beam evolution and consequently the strength of the wakefield at the time of injection can be controlled. This set of free parameters is used to optimize the injected charge and, in particular, the angular-spectral charge density of the witness bunches from the PWFA stage.

For an injected witness charge of about 30 pC there is a regime where a flattening of the longitudinal phase space is observed. This manifests itself in a reduced energy spread and an increased spectral charge density of the witness. The charge-dependent behavior of the witness' spectral charge density hints at beam loading as an explanation for this observation [70]. Witness electron bunches with low divergence, low energy spread, and high spectral charge density are produced in a fraction of the shots. The reproducibility of such beams is limited by the shot-to-shot fluctuations of the injected witness charge. Figure 4(b) depicts an example for a separation of LWFA and PWFA of 19 mm. The peak energy of this witness bunch is 162 MeV. The bunch charge of the narrow band bunch is (31 ± 5) pC. Its FWHM and rms (from Gaussian fit to spectrum) energy spread is 5.6 and 2.4 MeV, respectively, approaching the energy resolution of the nonimaging dipole spectrometer [71]. The beams thus exhibit a very good, low energy spread-to-gain ratio of 3.5%, commonly defined as the FWHM energy spread of the witness divided by its energy gain. This is 5 times less than the relative energy spread of the driver in this experiment (18%).

Furthermore, we observe that these witness bunches have an average divergence of 0.28 mrad (rms of super-Gaussian fit, 0.6 mrad FWHM), only. Using pure LWFA, similarly small divergences were only observed for near-GeV beams [72]. Since the beam divergence is given by the ratio of transverse to longitudinal momentum, this hints at a competitively small beam emittance, as we elaborate on later. Combined with its charge of 30 pC, this yields an
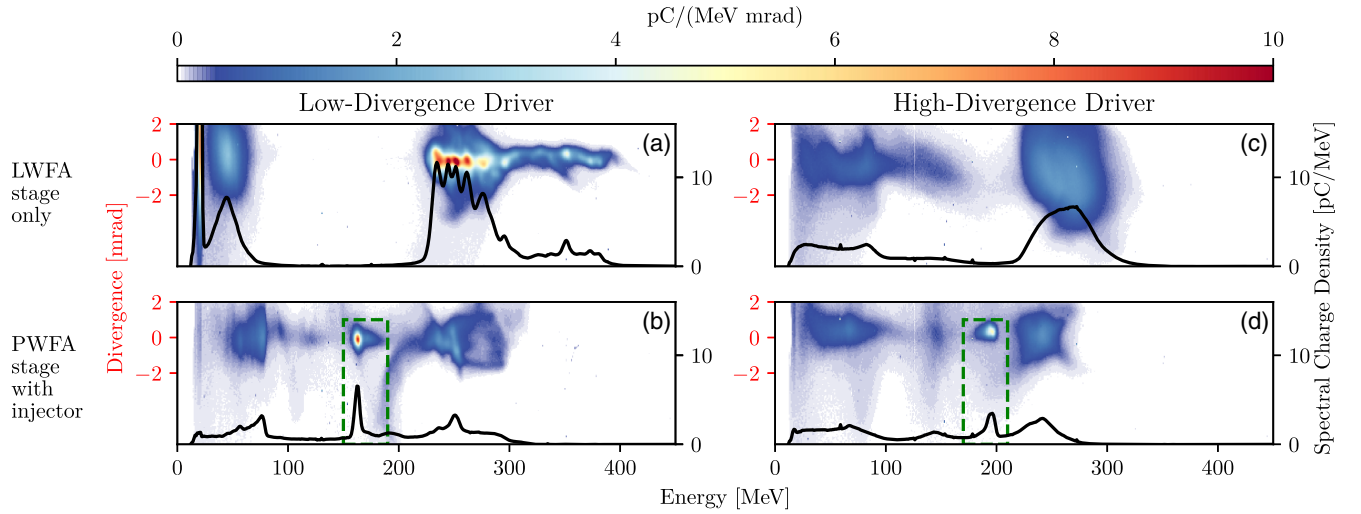
FIG. 4.   Increase of angular-spectral charge density in the PWFA stage. (a) Typical spectrum of a low-divergence LWFA-generated drive beam with 640 pC bunch charge in the high-energy feature and an average divergence of 0.41 mrad (rms of super-Gaussian fit), leading to an angular-spectral charge density of 5 pC/(MeV μsr). (b) Spectrum after the PWFA stage with optimized beam loading for high charge density of the witness beam. Because of the lower divergence of 0.28 mrad (rms of super-Gaussian fit) of the 30 pC witness beam, its angular-spectral charge density is 40% higher than the driver [7 pC/(MeV μsr)]. (c) Typical LWFA-driver spectrum for the high-divergence case (1.2 mrad, rms of super-Gaussian fit). Using this beam with a charge of 400 pC and an angular-spectral charge density of only 0.4 pC/(MeV μsr), a witness beam (d) with 0.22 mrad rms divergence, 20 pC charge, and an angular-spectral charge density of 6 pC/(MeV μsr) is generated.

angular-spectral charge density of 7 pC/(MeV μsr), which is approximately 40% denser than the drive beam. As seen both in simulations and in first experimental results already a slight improvement in terms of electron beam quality can enable further progress in realizing free-electron lasers [21,73–76]. Thus, the beams generated in our PWFA are very promising for various such applications. In particular, with a divergence after extraction of well below 1 mrad in combination with percent-level energy spread, the beams can be coupled into a beam line and transported without significant degradation [77].

Remarkably, the production of these dense, low-divergence witness beams is not limited to highly optimized, submillirad drive beams such as the one shown in Fig. 4(a), but is also seen in experiments with significantly more divergent LWFA beams as driver. Figure 4(c) shows a representative shot from a different dataset with the drive bunch containing 400 pC, a divergence of 1.2 mrad (rms of super-Gaussian fit) and thus with a much lower angular-spectral charge density of 0.4 pC/(MeV μsr) at 270 MeV. These beams can still drive a plasma wakefield and, as shown in Fig. 4(d), yield high-quality witness bunches with a similarly small divergence of 0.22 mrad (rms of super-Gaussian fit) and 2.3% (rms of Gaussian fit) energy spread. At a charge of 20 pC the angular-spectral charge density of these witness bunches evaluates to 6 pC/(MeV μsr) at 195 MeV. This is an order of magnitude denser than the driver. The witness properties, in particular its angular-spectral charge density, thus appear to be largely insensitive to the driver divergence in an interval spanning more than

one order of magnitude [79]. The similar, small divergence of the witness beams in both scenarios indicates that the injected electrons mainly carry the intrinsic transverse momentum spread of our injection method and are little affected by either the electron driver or the remainder of the laser pulse from the LWFA stage. In the following we establish reasonable upper and lower limits on the emittance of the witness beam.

Shock-injected electrons originate from the bubble sheath, and therefore have previously been transversely displaced by the driver. An upper limit for the divergence and emittance of the witness beam in this scheme can thus be calculated by the transverse momentum of the sheath electrons falling back onto axis at the rear of the bubble.

We estimate the order of magnitude of the intrinsic transverse momentum in our implementation of density down-ramp injection based on the simplified model derived above. From the transverse momentum betatron trajectories and the normalized emittance of the electron bunch are calculated [42]. For a driver current of 20 kA, a plasma density of $n_0 = 1 \times 10^{18}$ cm^{-3}, and a Lorentz factor of $\gamma = 300$, the upper limit for the divergence angle at the end of the longitudinal acceleration is $\sigma_\theta = 4$ mrad. At this point the betatron amplitude of the electrons defining the contour of the phase-space ellipse is $\sigma_x = \sigma_\theta c/\omega_\beta = 0.5$ μm. Here $\omega_\beta = \omega_p/\sqrt{2\gamma}$ is the local betatron frequency and $\omega_p = \sqrt{e^2 n_0/\epsilon_0 m_e}$ the plasma frequency. These numbers yield an upper limit for the normalized emittance of

$$\epsilon_n < \gamma \sigma_\theta^{max} \sigma_x^{max} = 0.6 \text{ mm mrad}. \qquad (5)$$

The estimated divergence value of 4 mrad is more than 10 times larger than the measured divergence of the witness beam. This observation indicates a considerably smaller emittance due to less transverse momentum of the electrons at the position and time of injection. A damping of the transverse momentum can happen because of a transversely defocusing field of the on-axis density spike at the rear of the bubble [80] or because of the space-charge field of the injected electrons themselves effectively lowering the focusing fields inside the bubble while being injected [59].

A lower limit for the normalized emittance can be calculated from the measured free-space divergence, assuming that the transverse momentum is identical inside the wakefield and after extraction to free space. However, adiabatic matching of the witness beam divergence may occur in the density down ramp of the jet or in a possible transition from a blowout to a linear wakefield at the end of the acceleration process [81–83]. Thus, just assuming the measured free-space divergence to be indicative for the transverse momentum during the acceleration will likely underestimate the emittance [84]. We can also compare the theoretical estimates to high-resolution PIC simulations of down-ramp injection from the previous section, cf. Fig. 3(b). While these simulations only roughly approximate our experimental conditions, the emittance of the high-density part of the witness [42] fits well into our estimates with $\epsilon_n^{sim} \approx 0.25$ mm mrad. While these estimates hint at a small witness emittance that is independent from and lower than the driver's, additional diagnostics and measurements will be required to determine its actual value.

V. CONCLUSION AND OUTLOOK

In the present paper, we provide first evidence that combined LWFA-PWFA offers a path to generate witness beams with improved quality parameters as compared to a single-stage LWFA. We have investigated the energy stability of electron acceleration in a staged LWFA-PWFA with an optically induced density down ramp in the PWFA. The energy of the witness beam is largely insensitive to the energy, energy spread, and emittance of the drive bunch produced in the LWFA stage. Furthermore, the addition of a subsequent PWFA stage for injection and acceleration makes use of the intrinsic resilience of beam-driven wakefields to shot-to-shot variations of the drive beam charge. This behavior is contrary to LWFA, where the electron properties are strongly correlated to variations of the driving laser pulse energy and focus position [28]. In our staged scheme we observe similar shot-to-shot stability as in PWFA experiments driven by conventional rf accelerators, despite substantially stronger fluctuations of the driver in terms of charge and energy. Simulations show that in our hybrid scheme, the PWFA stage can generate electron beams with higher stability than the driving

LWFA itself. Our simulations suggest that the stability of the witness energy can be increased even beyond the stability of an unloaded wakefield when controlling the amount of injected charge. For this, more stable targets (e.g., gas cells) should be employed. Furthermore, the injection and acceleration need to be further decoupled to better control the amount of injected charge (e.g., in a plasma photocathode scheme). For highest stability of the witness energy these measures in the PWFA stage can be combined with more stable drive bunches produced via active stabilization of the laser driving the LWFA [28].

The position of the optically generated density down ramp in the PWFA stage is very stable and thus one major source of witness energy fluctuations is eliminated. Furthermore, injection at such planar optically generated shocks and acceleration in the PWFA stage is very robust against pointing fluctuations of the laser driver and as a result the LWFA electron beam. This is because both the jet dimension and the transverse extent of the astigmatic focus of the injector laser beam in the PWFA stage are much larger than the typical transverse jitter of the drive laser. The presented laser-blocker-free setup is essentially self-aligning because the spent laser driver acting as an ionizer for the PWFA stage always propagates sufficiently collinearly with the electron beam.

Without the laser blocker and by controlling the amount of injected witness charge, we achieve narrow band witness spectra via beam loading. The angular-spectral charge density of PWFA beams injected at an optically induced density down ramp exceeds the one of the drive beam being used. We thus demonstrate that an additional PWFA stage with internal injection driven by a LWFA acts as a beam-quality transformer.

The energy transfer efficiency is higher than in previous PWFA experiments. The ratio of the integrated energy of the witness to the integrated energy of the incident drive bunch is up to 10%. Furthermore, a high beam quality of the witness beam and simultaneously a high energy gain of 65% of the initial electron energy of the driver has been shown. However, there are different limiting factors for achieving a witness energy that exceeds the driver energy in our specific experimental implementation of the PWFA stage. As seen in Fig. 3(a), the effective acceleration length is limited to ~1.5 mm in our first set of experiments, because of the long density down ramp and the associated dephasing of the witness bunch in the PWFA target. Also, under our experimental conditions the injected witness charge should be limited to a few 10 pC to avoid strong beam loading, which limits the energy gain in the PWFA. Furthermore, due to the free-space drift between LWFA and PWFA the drive bunch is not matched into the PWFA plasma. Thus, the emittance of the drive beam degraded when entering the PWFA [42] and its full ability to drive strong wakefields is not exploited. This can be addressed by implementing a low-density passive plasma

lens between both stages. Or at least mitigated by a reduction in stage separation, which in the case without blocker tape comes at the expense of a stronger remaining laser driver from the LWFA.

Because of the low free-space divergence and low energy spread of our witness beams, their emittance growth during propagation in free space is smaller than for most beams reported in previous wakefield accelerator experiments. Thus, they are suited for applications involving an electron beam transport line. In follow-up experiments a careful and full assessment of the overall and slice emittance has to be done to asses the suitability of these beams for a free-electron laser. Furthermore, we plan to implement advanced injection schemes such as the plasma photocathode [32] or wake-induced ionization injection [33,34] that promise a further reduction of the witness emittance.

The two-stage LWFA-PWFA scheme is particularly interesting for facilities offering hundred terawatt- to petawatt-scale laser power that can generate electron beams with nanocoulomb-class beam charge and tens of kiloampere peak current. Energy transfer efficiency and electron-energy gain shown in this paper encourage us to consider a final PWFA stage with internal witness injection as a beam quality and stability booster after a single or multiple LWFA stages. In the latter case this would relax the demands on emittance preservation in the LWFAs by far. This scheme may be a promising future research direction for high-energy physics applications of wakefield accelerators.

ACKNOWLEDGMENTS

[1] E. Esarey, C. B. Schroeder, and W. P. Leemans, *Physics of Laser-Driven Plasma-Based Electron Accelerators*, Rev. Mod. Phys. **81**, 1229 (2009).

[2] V. Malka, *Laser Plasma Accelerators*, Phys. Plasmas **19**, 055501 (2012).

[3] J. Wenz, A. Döpp, K. Khrennikov, S. Schindler, M. F. Gilljohann, H. Ding, J. Götzfried, A. Buck, J. Xu, M. Heigoldt, W. Helml, L. Veisz, and S. Karsch, *Dual-Energy Electron Beams from a Compact Laser-Driven Accelerator*, Nat. Photonics **13**, 263 (2019).

[4] K. Oubrerie, A. Leblanc, O. Kononenko, R. Lahaye, I. A. Andriyash, J. Gautier, J.-P. Goddet, L. Martelli, A. Tafzi, K. T. Phuoc, S. Smartsev, and C. Thaury, *Controlled Acceleration of GeV Electron Beams in an All-Optical Plasma Waveguide*, Light Sci. Appl. **11**, 180 (2022).

[5] M. Kirchen, S. Jalas, P. Messner, P. Winkler, T. Eichner, L. Hübner, T. Hülsenbusch, L. Jeppe, T. Parikh, M. Schnepp, and A. R. Maier, *Optimal Beam Loading in a Laser-Plasma Accelerator*, Phys. Rev. Lett. **126**, 174801 (2021).

[6] M. S. Bloom, M. J. V. Streeter, S. Kneip, R. A. Bendoyro, O. Cheklov, J. M. Cole, A. Döpp, C. J. Hooker, J. Holloway, J. Jiang, N. C. Lopes, H. Nakamura, P. A. Norreys, P. P. Rajeev, D. R. Symes, J. Schreiber, J. C. Wood, M. Wing, Z. Najmudin, and S. P. D. Mangles, *Bright X-Ray Radiation from Plasma Bubbles in an Evolving Laser Wakefield Accelerator*, Phys. Rev. Accel. Beams **23**, 061301 (2020).

[7] M. B. Schwab, E. Siminos, T. Heinemann, D. Ullmann, F. Karbstein, S. Kuschel, A. Savert, M. Yeung, D. Hollatz, A. Seidel, J. Cole, S. P. D. Mangles, B. Hidding, M. Zepf, S. Skupin, and M. C. Kaluza, *Visualization of Relativistic Laser Pulses in Underdense Plasma*, Phys. Rev. Accel. Beams **23**, 032801 (2020).

[8] A. E. Hussein, N. Senabulya, Y. Ma, M. J. V. Streeter, B. Kettle, S. J. D. Dann, F. Albert, N. Bourgeois, S. Cipiccia, J. M. Cole *et al.*, *Laser-Wakefield Accelerators for High-Resolution X-Ray Imaging of Complex Microstructures*, Sci. Rep. **9**, 3249 (2019).

[9] N. Lemos, P. King, J. L. Shaw, A. L. Milder, K. A. Marsh, A. Pak, B. B. Pollock, C. Goyon, W. Schumaker, A. M. Saunders *et al.*, *X-Ray Sources Using a Picosecond Laser Driven Plasma Accelerator*, Phys. Plasmas **26**, 083110 (2019).

[10] A. J. Gonsalves, K. Nakamura, J. Daniels, C. Benedetti, C. Pieronek, T. C. H. de Raadt, S. Steinke, J. H. Bin, S. S. Bulanov, J. van Tilborg *et al.*, *Petawatt Laser Guiding and Electron Beam Acceleration to 8 GeV in a Laser-Heated Capillary Discharge Waveguide*, Phys. Rev. Lett. **122**, 084801 (2019).

[11] C. Aniculaesei, V. B. Pathak, K. H. Oh, P. K. Singh, B. R. Lee, C. I. Hojbota, T. G. Pak, E. Brunetti, B. J. Yoo, J. H. Sung, S. K. Lee, H. T. Kim, and C. H. Nam, *Proof-of-Principle Experiment for Nanoparticle-Assisted Laser Wakefield Electron Acceleration*, Phys. Rev. Appl. **12,** 044041 (2019).

[12] J. Götzfried, A. Döpp, M. F. Gilljohann, F. M. Foerster, H. Ding, S. Schindler, G. Schilling, A. Buck, L. Veisz, and S. Karsch, *Physics of High-Charge Electron Beams in Laser-Plasma Wakefields*, Phys. Rev. X **10,** 041015 (2020).

[13] J. P. Couperus, R. Pausch, A. Köhler, O. Zarini, J. M. Krämer, M. Garten, A. Huebl, R. Gebhardt, U. Helbig, S. Bock, K. Zeil, A. Debus, M. Bussmann, U. Schramm, and A. Irman, *Demonstration of a Beam Loaded Nanocoulomb-Class Laser Wakefield Accelerator*, Nat. Commun. **8,** 487 (2017).

[14] M. Heigoldt, A. Popp, K. Khrennikov, J. Wenz, S. W. Chou, S. Karsch, S. I. Bajlekov, S. M. Hooker, and B. Schmidt, *Temporal Evolution of Longitudinal Bunch Profile in a Laser Wakefield Accelerator*, Phys. Rev. ST Accel. Beams **18,** 121302 (2015).

[15] A. Buck, M. Nicolai, K. Schmid, C. M. S. Sears, A. Sävert, J. M. Mikhailova, F. Krausz, M. C. Kaluza, and L. Veisz, *Real-Time Observation of Laser-Driven Electron Acceleration*, Nat. Phys. **7,** 543 (2011).

[16] O. Lundh, J. Lim, C. Rechatin, L. Ammoura, A. Ben-Ismail, X. Davoine, G. Gallot, J. P. Goddet, E. Lefebvre, V. Malka, and J. Faure, *Few Femtosecond, Few Kiloampere Electron Bunch Produced by a Laser–Plasma Accelerator*, Nat. Phys. **7,** 219 (2011).

[17] S. Kneip, C. McGuffey, J. L. Martins, S. F. Martins, C. Bellei, V. Chvykov, F. Dollar, R. Fonseca, C. Huntington, G. Kalintchenko *et al.*, *Bright Spatially Coherent Synchrotron X-Rays from a Table-Top Source*, Nat. Phys. **6,** 980 (2010).

[18] J. Wenz, S. Schleede, K. Khrennikov, M. Bech, P. Thibault, M. Heigoldt, F. Pfeiffer, and S. Karsch, *Quantitative X-Ray Phase-Contrast Microtomography from a Compact Laser-Driven Betatron Source*, Nat. Commun. **6,** 7568 (2015).

[19] A. Koehler, R. Pausch, M. Bussmann, J. P. Couperus Cabadağ, A. Debus, J. M. Krämer, S. Schöbel, O. Zarini, U. Schramm, and A. Irman, *Restoring Betatron Phase Coherence in a Beam-Loaded Laser-Wakefield Accelerator*, Phys. Rev. Accel. Beams **24,** 091302 (2021).

[20] W. T. Wang, W. T. Li, J. S. Liu, Z. J. Zhang, R. Qi, C. H. Yu, J. Q. Liu, M. Fang, Z. Y. Qin, C. Wang, Y. Xu, F. X. Wu, Y. X. Leng, R. X. Li, and Z. Z. Xu, *High-Brightness High-Energy Electron Beams from a Laser Wakefield Accelerator via Energy Chirp Control*, Phys. Rev. Lett. **117,** 124801 (2016).

[21] W. Wang, K. Feng, L. Ke, C. Yu, Y. Xu, R. Qi, Y. Chen, Z. Qin, Z. Zhang, M. Fang, J. Liu, K. Jiang, H. Wang, C. Wang, X. Yang, F. Wu, Y. Leng, J. Liu, R. Li, and Z. Xu, *Free-Electron Lasing at 27 Nanometres Based on a Laser Wakefield Accelerator*, Nature (London) **595,** 516 (2021).

[22] A. Döpp, C. Thaury, E. Guillaume, F. Massimo, A. Lifschitz, I. Andriyash, J.-P. Goddet, A. Tazfi, K. Ta Phuoc, and V. Malka, *Energy-Chirp Compensation in a Laser Wakefield Accelerator*, Phys. Rev. Lett. **121,** 074802 (2018).

[23] M. J. V. Streeter, S. Kneip, M. S. Bloom, R. A. Bendoyro, O. Chekhlov, A. E. Dangor, A. Döpp, C. J. Hooker, J. Holloway, J. Jiang, N. C. Lopes, H. Nakamura, P. A. Norreys, C. A. J. Palmer, P. P. Rajeev, J. Schreiber, D. R. Symes, M. Wing, S. P. D. Mangles, and Z. Najmudin, *Observation of Laser Power Amplification in a Self-Injecting Laser Wakefield Accelerator*, Phys. Rev. Lett. **120,** 254801 (2018).

[24] S. Corde, C. Thaury, A. Lifschitz, G. Lambert, K. T. Phuoc, X. Davoine, R. Lehe, D. Douillet, A. Rousse, and V. Malka, *Observation of Longitudinal and Transverse Self-Injections in Laser-Plasma Accelerators*, Nat. Commun. **4,** 1501 (2013).

[25] E. Brunetti, R. P. Shanks, G. G. Manahan, M. R. Islam, B. Ersfeld, M. P. Anania, S. Cipiccia, R. C. Issac, G. Raj, G. Vieux, G. H. Welsh, S. M. Wiggins, and D. A. Jaroszynski, *Low Emittance, High Brilliance Relativistic Electron Beams from a Laser-Plasma Accelerator*, Phys. Rev. Lett. **105,** 215007 (2010).

[26] R. Weingartner, S. Raith, A. Popp, S. Chou, J. Wenz, K. Khrennikov, M. Heigoldt, A. Maier, N. Kajumba, M. Fuchs, B. Zeitler, F. Krausz, S. Karsch, and F. Gruner, *Ultralow Emittance Electron Beams from a Laser-Wakefield Accelerator*, Phys. Rev. ST Accel. Beams **15,** 111302 (2012).

[27] G. Golovin, S. Banerjee, C. Liu, S. Chen, J. Zhang, B. Zhao, P. Zhang, M. Veale, M. Wilson, P. Seller, and D. Umstadter, *Intrinsic Beam Emittance of Laser-Accelerated Electrons Measured by X-Ray Spectroscopic Imaging*, Sci. Rep. **6,** 24622 (2016).

[28] A. R. Maier, N. M. Delbos, T. Eichner, L. Hübner, S. Jalas, L. Jeppe, S. W. Jolly, M. Kirchen, V. Leroux, P. Messner, M. Schnepp, M. Trunk, P. A. Walker, C. Werle, and P. Winkler, *Decoding Sources of Energy Variability in a Laser-Plasma Accelerator*, Phys. Rev. X **10,** 031039 (2020).

[29] C. A. Lindstrøm, *Staging of Plasma-Wakefield Accelerators*, Phys. Rev. Accel. Beams **24,** 014801 (2021).

[30] G. Raj, O. Kononenko, M. F. Gilljohann, A. Doche, X. Davoine, C. Caizergues, Y.-Y. Chang, J. P. Couperus Cabadağ, A. Debus, H. Ding *et al.*, *Probing Ultrafast Magnetic-Field Generation by Current Filamentation Instability in Femtosecond Relativistic Laser-Matter Interactions*, Phys. Rev. Res. **2,** 023123 (2020).

[31] C. Joshi, S. Corde, and W. B. Mori, *Perspectives on the Generation of Electron Beams from Plasma-Based Accelerators and Their Near and Long Term Applications*, Phys. Plasmas **27,** 070602 (2020).

[32] B. Hidding, G. Pretzler, J. B. Rosenzweig, T. Königstein, D. Schiller, and D. L. Bruhwiler, *Ultracold Electron Bunch Generation via Plasma Photocathode Emission and Acceleration in a Beam-Driven Plasma Blowout*, Phys. Rev. Lett. **108,** 035001 (2012).

[33] A. Martinez de la Ossa, J. Grebenyuk, T. Mehrling, L. Schaper, and J. Osterhoff, *High-Quality Electron Beams from Beam-Driven Plasma Accelerators by Wakefield-Induced Ionization Injection*, Phys. Rev. Lett. **111,** 245003 (2013).

[34] A. Martinez de la Ossa, T. J. Mehrling, L. Schaper, M. J. V. Streeter, and J. Osterhoff, *Wakefield-Induced Ionization Injection in Beam-Driven Plasma Accelerators*, Phys. Plasmas **22,** 093107 (2015).

[35] I. Blumenfeld, C. E. Clayton, F. J. Decker, M. J. Hogan, C. K. Huang, R. Ischebeck, R. Iverson, C. Joshi, T. Katsouleas, N. Kirby, W. Lu, K. A. Marsh, W. B. Mori, P. Muggli, E. Oz, R. H. Siemann, D. Walz, and M. M. Zhou, *Energy Doubling of 42 GeV Electrons in a Metre-Scale Plasma Wakefield Accelerator*, Nature (London) **445**, 741 (2007).

[36] M. Litos, E. Adli, W. An, C. I. Clarke, C. E. Clayton, S. Corde, J. P. Delahaye, R. J. England, A. S. Fisher, J. Frederico *et al.*, *High-Efficiency Acceleration of an Electron Beam in a Plasma Wakefield Accelerator*, Nature (London) **515**, 92 (2014).

[37] C. A. Lindstrøm, J. M. Garland, S. Schröder, L. Boulton, G. Boyle, J. Chappell, R. D'Arcy, P. Gonzalez, A. Knetsch, V. Libov, G. Loisch, A. Martinez de la Ossa, P. Niknejadi, K. Põder, L. Schaper, B. Schmidt, B. Sheeran, S. Wesch, J. Wood, and J. Osterhoff, *Energy-Spread Preservation and High Efficiency in a Plasma-Wakefield Accelerator*, Phys. Rev. Lett. **126**, 014801 (2021).

[38] E. Adli, A. Ahuja, O. Apsimon, R. Apsimon, A. M. Bachmann, D. Barrientos, F. Batsch, J. Bauche, V. K. B. Olsen, M. Bernardini *et al.*, *Acceleration of Electrons in the Plasma Wakefield of a Proton Bunch*, Nature (London) **561**, 363 (2018).

[39] M. F. Gilljohann, H. Ding, A. Döpp, J. Götzfried, S. Schindler, G. Schilling, S. Corde, A. Debus, T. Heinemann, B. Hidding, S. M. Hooker, A. Irman, O. Kononenko, T. Kurz, A. Martinez de la Ossa, U. Schramm, and S. Karsch, *Direct Observation of Plasma Waves and Dynamics Induced by Laser-Accelerated Electron Beams*, Phys. Rev. X **9**, 011046 (2019).

[40] T. Kurz, T. Heinemann, M. F. Gilljohann, Y. Y. Chang, J. P. C. Cabadağ, A. Debus, O. Kononenko, R. Pausch, S. Schöbel, R. W. Assmann *et al.*, *Demonstration of a Compact Plasma Accelerator Powered by Laser-Accelerated Electron Beams*, Nat. Commun. **12**, 2895 (2021).

[41] We introduce the angular-spectral charge density as a figure of merit for the beam quality. Its mathematical definition can be found in the Supplemental Material [42].

[42] See Supplemental Material at http://link.aps.org/supplemental/10.1103/PhysRevX.12.041016 for additional information on the experimental setup, parameters for simulations, and details on data analysis.

[43] For further details on the laser system, see Supplemental Material [42], Pt. A1.

[44] Because of the larger distance of the beam axis from the nozzle, the gas profile has no plateau region.

[45] C. Thaury, E. Guillaume, A. Lifschitz, K. Ta Phuoc, M. Hansson, G. Grittani, J. Gautier, J. P. Goddet, A. Tafzi, O. Lundh, and V. Malka, *Shock Assisted Ionization Injection in Laser-Plasma Accelerators*, Sci. Rep. **5**, 16310 (2015).

[46] J. P. Couperus Cabadağ, R. Pausch, S. Schöbel, M. Bussmann, Y.-Y. Chang, S. Corde, A. Debus, H. Ding, A. Döpp, F. M. Foerster *et al.*, *Gas-Dynamic Density Downramp Injection in a Beam-Driven Plasma Wakefield Accelerator*, Phys. Rev. Res. **3**, L042005 (2021).

[47] R. J. Shalloo, C. Arran, L. Corner, J. Holloway, J. Jonnerby, R. Walczak, H. M. Milchberg, and S. M. Hooker, *Hydrodynamic Optical-Field-Ionized Plasma Channels*, Phys. Rev. E **97**, 053203 (2018).

[48] R. J. Shalloo, C. Arran, A. Picksley, A. von Boetticher, L. Corner, J. Holloway, G. Hine, J. Jonnerby, H. M. Milchberg, C. Thornton, R. Walczak, and S. M. Hooker, *Low-Density Hydrodynamic Optical-Field-Ionized Plasma Channels Generated with an Axicon Lens*, Phys. Rev. Accel. Beams **22**, 041302 (2019).

[49] J. Faure, C. Rechatin, O. Lundh, L. Ammoura, and V. Malka, *Injection and Acceleration of Quasimonoenergetic Relativistic Electron Beams Using Density Gradients at the Edges of a Plasma Channel*, Phys. Plasmas **17**, 083107 (2010).

[50] S. Fourmaux, K. Ta Phuoc, P. Lassonde, S. Corde, G. Lebrun, V. Malka, A. Rousse, and J. C. Kieffer, *Quasi-Monoenergetic Electron Beams Production in a Sharp Density Transition*, Appl. Phys. Lett. **101**, 111106 (2012).

[51] P. Brijesh, C. Thaury, K. T. Phuoc, S. Corde, G. Lambert, V. Malka, S. P. D. Mangles, M. Bloom, and S. Kneip, *Tuning the Electron Energy by Controlling the Density Perturbation Position in Laser Plasma Accelerators*, Phys. Plasmas **19**, 063104 (2012).

[52] A detailed description of the HOFI shocks can be found in the Supplemental Material [42], Pt. B1.

[53] K. K. Swanson, H. E. Tsai, S. K. Barber, R. Lehe, H. S. Mao, S. Steinke, J. van Tilborg, K. Nakamura, C. G. R. Geddes, C. B. Schroeder, E. Esarey, and W. P. Leemans, *Control of Tunable, Monoenergetic Laser-Plasma-Accelerated Electron Beams Using a Shock-Induced Density Downramp Injector*, Phys. Rev. Accel. Beams **20**, 051301 (2017).

[54] L. Fan-Chiang, H. S. Mao, H. E. Tsai, T. Ostermayr, K. K. Swanson, S. K. Barber, S. Steinke, J. van Tilborg, C. G. R. Geddes, and W. P. Leemans, *Gas Density Structure of Supersonic Flows Impinged on by Thin Blades for Laser–Plasma Accelerator Targets*, Phys. Fluids **32**, 066108 (2020).

[55] T. Kurz, J. P. Couperus, J. M. Krämer, H. Ding, S. Kuschel, A. Köhler, O. Zarini, D. Hollatz, D. Schinkel, R. D'Arcy, J.-P. Schwinkendorf, J. Osterhoff, A. Irman, U. Schramm, and S. Karsch, *Calibration and Cross-Laboratory Implementation of Scintillating Screens for Electron Bunch Charge Determination*, Rev. Sci. Instrum. **89**, 093303 (2018).

[56] A. Knetsch, B. Sheeran, L. Boulton, P. Niknejadi, K. Põder, L. Schaper, M. Zeng, S. Bohlen, G. Boyle, T. Brümmer *et al.*, *Stable Witness-Beam Formation in a Beam-Driven Plasma Cathode*, Phys. Rev. Accel. Beams **24**, 101302 (2021).

[57] D. Ullmann, P. Scherkl, A. Knetsch, T. Heinemann, A. Sutherland, A. F. Habib, O. S. Karger, A. Beaton, G. G. Manahan, A. Deng, G. Andonian, M. D. Litos, B. D. OShea, J. R. Cary, M. J. Hogan, V. Yakimenko, J. B. Rosenzweig, and B. Hidding, *All-Optical Density Downramp Injection in Electron-Driven Plasma Wakefield Accelerators*, Phys. Rev. Res. **3**, 043163 (2021).

[58] A more careful derivation taking into account the relativistic motion of the plasma electrons and the magnetic field in the blowout [59] yields $E_{ion}(r) = -en_0 r/4\epsilon_0$ and $r_b = \sqrt{2I_0/\pi ec n_0}$. Thus, the same functional dependence but modified constants.

[59] A. Martinez de la Ossa, Z. Hu, M. J. V. Streeter, T. J. Mehrling, O. Kononenko, B. Sheeran, and J. Osterhoff, *Optimizing Density Down-Ramp Injection for Beam-Driven Plasma Wakefield Accelerators*, Phys. Rev. Accel. Beams **20,** 091301 (2017).

[60] K. V. Lotov, *Efficient Operating Mode of the Plasma Wakefield Accelerator*, Phys. Plasmas **12,** 053105 (2005).

[61] This number includes all contributions to the variation of witness energy. The "=" sign would apply if the variation in witness energy is only due to charge variations of the driver.

[62] R. Lehe, M. Kirchen, I. A. Andriyash, B. B. Godfrey, and J.-L. Vay, *A Spectral, Quasi-Cylindrical and Dispersion-Free Particle-In-Cell Algorithm*, Comput. Phys. Commun. **203,** 66 (2016).

[63] Note that, e.g., Refs. [36,37] use a different definition for the energy transfer efficiency, namely, the driver's energy loss $\Delta E_{\mathrm{driver}}$ instead of the initial driver energy in the denominator ($\tilde{\eta} = \Delta E_{\mathrm{witness}}/\Delta E_{\mathrm{driver}}$). Their definition thus yields high-efficiency figures even far from driver depletion.

[64] This efficiency was measured in sets with less stable witness formation. A representative shot is presented in the Supplemental Material [42].

[65] M. Litos, E. Adli, J. M. Allen, W. An, C. I. Clarke, S. Corde, C. E. Clayton, J. Frederico, S. J. Gessner, S. Z. Green, M. J. Hogan, C. Joshi, W. Lu, K. A. Marsh, W. B. Mori, M. Schmeltz, N. Vafaei-Najafabadi, and V. Yakimenko, *9 GeV Energy Gain in a Beam-Driven Plasma Wakefield Accelerator*, Plasma Phys. Controlled Fusion **58,** 034017 (2016).

[66] A. Martinez de la Ossa, R. W. Assmann, M. Bussmann, S. Corde, J. P. Couperus Cabadağ, A. Debus, A. Döpp, A. Ferran Pousa, M. F. Gilljohann, T. Heinemann, B. Hidding, A. Irman, S. Karsch, O. Kononenko, T. Kurz, J. Osterhoff, R. Pausch, S. Schöbel, and U. Schramm, *Hybrid LWFA-PWFA Staging as a Beam Energy and Brightness Transformer: Conceptual Design and Simulations*, Phil. Trans. R. Soc. A **377,** 20180175 (2019).

[67] A more detailed definition of the angular-spectral charge density and a description of the analysis can be found in the Supplemental Material [42].

[68] C. Zhang, C.-K. Huang, K. A. Marsh, X. L. Xu, F. Li, M. Hogan, V. Yakimenko, S. Corde, W. B. Mori, and C. Joshi, *Effect of Fluctuations in the Down Ramp Plasma Source Profile on the Emittance and Current Profile of the Self-Injected Beam in a Plasma Wakefield Accelerator*, Phys. Rev. Accel. Beams **22,** 111301 (2019).

[69] See the Supplemental Material [42] for a detailed discussion of the influence of the jet separation, different injection conditions, and low-energy features in the spectra.

[70] A comparison of the spectral charge density for different amount of injected charge can be found in the Supplemental Material [42].

[71] In our specific dipole spectrometer setup a monoenergetic electron bunch at 162 MeV with a FWHM divergence of 0.6 mrad appears to have an energy spread of 3.5 MeV (FWHM).

[72] L. T. Ke, K. Feng, W. T. Wang, Z. Y. Qin, C. H. Yu, Y. Wu, Y. Chen, R. Qi, Z. J. Zhang, Y. Xu, X. J. Yang, Y. X. Leng, J. S. Liu, R. X. Li, and Z. Z. Xu, *Near-GeV Electron Beams at a Few Per-Mille Level from a Laser Wakefield Accelerator via Density-Tailored Plasma*, Phys. Rev. Lett. **126,** 214801 (2021).

[73] R. Lehe, *Improvement of the Quality of Laser-Wakefield Accelerators*, Ph.D. thesis, Ecole Polytechnique, 2014.

[74] M. E. Couprie, *Panorama of New Generation of Accelerator Based Short Wavelength Coherent Light Sources*, Nucl. Instrum. Methods Phys. Res., Sect. B **364,** 4 (2015).

[75] T. André, I. A. Andriyash, A. Loulergue, M. Labat, E. Roussel, A. Ghaith, M. Khojoyan, C. Thaury, M. Valléau, F. Briquez *et al.*, *Control of Laser Plasma Accelerated Electrons for Light Sources*, Nat. Commun. **9,** 1334 (2018).

[76] A. R. Maier, A. Meseck, S. Reiche, C. B. Schroeder, T. Seggebrock, and F. Gruner, *Demonstration Scheme for a Laser-Plasma-Driven Free-Electron Laser*, Phys. Rev. X **2,** 031019 (2012).

[77] Beam degradation due to chromatic beam transport can alternatively be described as a growth of normalized emittance during free-space propagation. Following the description by Migliorati *et al.* [78], the normalized emittance evolution of a beam with energy spread and divergence is given by $\epsilon_{n,\mathrm{rms}} = \gamma\sqrt{\sigma_\gamma^2\sigma_{x'}^4(z-z_0)^2 + \epsilon_{\mathrm{rms}}}$. The emittance growth for our beam parameters evaluates to 0.30 mm mrad per 1 m of free-space propagation.

[78] M. Migliorati, A. Bacci, C. Benedetti, E. Chiadroni, M. Ferrario, A. Mostacci, L. Palumbo, A. R. Rossi, L. Serafini, and P. Antici, *Intrinsic Normalized Emittance Growth in Laser-Driven Electron Accelerators*, Phys. Rev. ST Accel. Beams **16,** 011302 (2013).

[79] Dedicated simulations to investigate the influence of the driver divergence and emittance can be found in the Supplemental Material [42].

[80] X. L. Xu, F. Li, W. An, T. N. Dalichaouch, P. Yu, W. Lu, C. Joshi, and W. B. Mori, *High Quality Electron Bunch Generation Using a Longitudinal Density-Tailored Plasma-Based Accelerator in the Three-Dimensional Blowout Regime*, Phys. Rev. Accel. Beams **20,** 111303 (2017).

[81] T. Mehrling, J. Grebenyuk, F. S. Tsung, K. Floettmann, and J. Osterhoff, *Transverse Emittance Growth in Staged Laser-Wakefield Acceleration*, Phys. Rev. ST Accel. Beams **15,** 111303 (2012).

[82] K. Floettmann, *Adiabatic Matching Section for Plasma Accelerated Beams*, Phys. Rev. ST Accel. Beams **17,** 054402 (2014).

[83] R. Ariniello, C. E. Doss, K. Hunt-Stone, J. R. Cary, and M. D. Litos, *Transverse Beam Dynamics in a Plasma Density Ramp*, Phys. Rev. Accel. Beams **22,** 041304 (2019).

[84] Such a calculation yields a rms radius of the betatron motion of $\sigma_x^{\min} = 0.4\ \mu$m and a normalized emittance of $\epsilon_n > \gamma\sigma_\theta^{\min}\sigma_x^{\min} = 0.004$ mm mrad.